energies

MDPI

Article

Multi-Fault Diagnosis of Three-Phase Four-Wire Inverter Based on Fuzzy Logic

Jian Huang, Yuan Sun *, Heping Fu, Guan Wang, Zuosheng Yin, Kai Cui and Chao Zhang

Beijing Institute of Automation Control Equipment, No.17 Yungang West Road, Fengtai District, Beijing 100074, China; huangjian421@126.com (J.H.); 18811385380@163.com (H.F.); wangguanhit@163.com (G.W.); yinzuosheng0102@163.com (Z.Y.); cuikai1881275@163.com (K.C.); 18117026@bjtu.edu.cn (C.Z.)

* Correspondence: yuansun@bjtu.edu.cn

Abstract

In modern power systems such as new energy generation and smart grids, inverters serve as core equipment for electrical energy conversion and transmission. Their operational reliability directly impacts system power supply quality and safety stability. Currently, research on inverter fault diagnosis technology primarily focuses on linear load conditions, with diagnostic method design and validation based on linear load characteristics. However, with the rapid advancement of power electronics technology, power electronic loads such as variable frequency drives, charging stations, and distributed power sources are increasingly prevalent in power systems. These loads exhibit nonlinear and time-varying characteristics under complex operating conditions, leading to a growing variety of inverter faults with significantly diversified and complex fault signatures. Traditional diagnostic methods fail to adapt to the unique characteristics of power electronic loads, making it difficult to accurately identify various faults. Consequently, they no longer meet the diagnostic demands of practical engineering scenarios. In addition, current diagnostic methods for open-circuit power transistors, intermittent faults, and sensor faults often employ different approaches, which consume significant controller resources and are prone to mutual interference, leading to false triggers. This paper takes a three-phase four-wire inverter as the research subject. Targeting the challenge of fault diagnosis under power electronic load conditions, it proposes a comprehensive diagnostic method capable of simultaneously diagnosing power switch open circuits, intermittent faults, and current sensor faults. First, the characteristics of various faults are analyzed. Subsequently, fault diagnosis variables are constructed using the actual arm voltage of the inverter and the ideal arm voltage. Logical rules for each type of fault are established, and diagnosis is performed through fuzzy logic inference. Finally, experiments validated the effectiveness of this fault diagnosis scheme, with open-circuit faults detected in less than 2 ms, intermittent faults in less than 0.5 ms, and sensor faults in less than 3 ms.

Keywords: sensor fault; open-circuit faults; intermittent fault; nonlinear load; fault diagnosis

Check for updates

Academic Editor: José Matas

Received: 18 May 2026
Revised: 8 June 2026
Accepted: 12 June 2026
Published: 23 June 2026

Copyright: © 2026 by the authors. Licensee MDPI, Basel, Switzerland. This article is an open access article distributed under the terms and conditions of the Creative Commons Attribution (CC BY) license.

1. Introduction

Two-level three-phase inverters find widespread application in diverse power equipment and power supply scenarios, attributed to their straightforward structure and superior operational capabilities. To satisfy the power demand of single-phase electrical devices while ensuring the reliable operation of three-phase power equipment, two-level three-phase four-wire inverters have been developed and extensively employed in areas

like distributed power generation [1], active power filters [2], and rail transit auxiliary inverters [3]. Statistical investigations reveal that power switch faults and sensor faults are the most common and damaging failures in power electronic inverters [4]. For switch short-circuit faults, a variety of detection and protection mechanisms integrated into the hardware can achieve prompt identification and protection [5]. On the other hand, inverter open-circuit faults, including those induced by fuse melting due to switch short-circuit faults in inverters fitted with fast fuses [6], are challenging to detect and safeguard against. Such open-circuit faults tend to accelerate the degradation of energy storage capacitors and inductors, reduce their operational lifespan, and undermine the stable operation of the entire system [7]. Thus, investigating open-circuit fault diagnosis techniques for inverters is of great significance in minimizing economic losses and improving the stability of drive systems.

Fault diagnosis methodologies are generally classified into two main categories: data-driven and circuit-driven approaches. Data-driven techniques primarily depend on the collection of extensive fault data and employ advanced signal processing methods or novel artificial intelligence models to accomplish fault diagnosis [8–10]. These approaches are associated with shortcomings such as the requirement for large-scale datasets, tedious data preprocessing workflows, and offline fault diagnosis durations that usually exceed one fundamental cycle. Circuit-driven methods are typically subdivided into voltage-based and current-based schemes. Voltage-based approaches mainly leverage the voltage difference between the reference voltage obtained from an accurate system model and the actually measured voltage to perform fault diagnosis [11–14]. Nevertheless, these methods demonstrate low efficiency and poor robustness when the system operates under light-load or no-load conditions. Current-based methods involve the direct utilization of current signals within the control system for fault analysis [15,16], without the need for additional hardware circuits. However, such techniques require the processing of current waveform signals, which results in substantial computational burden and high algorithm complexity. Relevant studies [17–19] have explored inverter fault diagnosis methods based on current observers. Observer-based methods exhibit insensitivity to load fluctuations and do not require extra measurement circuits, but they still have a strong reliance on precise mathematical modeling.

In addition to power switch faults in inverters, sensors are also highly prone to malfunctions. Current sensor faults may cause closed-loop systems to lose control, so the rapid diagnosis of current sensor faults is indispensable. Up to now, numerous researchers have carried out studies on current sensor faults [20–22], and the characteristics of these faults are analogous to those of power switch open-circuit faults.

Several research efforts have focused on the concurrent diagnosis of power switch open-circuit faults and current sensor faults. In [23], a diagnostic method based on the Luenberger observer is developed to identify open-circuit faults and sensor faults in two-level three-phase inverters. In [24], a current-based normalized Park vector approach combined with an adaptive threshold method is used for the diagnosis of open-circuit faults and current sensor faults. In [25], a synchronous diagnosis strategy based on a reduced-order observer is put forward, which transforms current sensor faults into generalized state vectors. This method adopts matrix transformation to decouple open-circuit faults from the inverter system states and current sensor faults, thereby achieving the diagnosis of IGBT faults and current sensor faults. However, the aforementioned studies fail to take DC-link voltage sensor faults into account. In [26], the stator flux linkage is used to identify speed sensor faults; a combination of a current-model-based stator flux linkage observer and a voltage-model-based stator flux linkage observer is used to diagnose DC-link voltage

sensor faults; and a current estimation method based on vector space decomposition is employed to identify IGBT faults.

Furthermore, the loads considered in the aforementioned literature are either induction motors or resistive loads. With the increasing adoption of power electronic loads or diode rectifier loads, a large number of harmonics are produced in the inverter's voltage and current [27,28]. When an open-circuit fault occurs in an inverter with nonlinear loads, the voltage and current of the non-faulty phases experience more severe distortion compared to those under linear load conditions. This situation is likely to lead to misdiagnosis, which affects the stable operation of the system and causes considerable damage to the inverter and associated equipment. Therefore, it is highly necessary to conduct research on fault diagnosis under nonlinear load conditions. In [2], the bridge arm voltage is constructed using the DC-link voltage and duty cycle, and the residual between this constructed voltage and the sampled voltage is utilized to realize open-circuit fault diagnosis of active power filters. However, this diagnostic method is vulnerable to DC-link voltage fluctuations and sampling spikes, resulting in poor robustness.

Although the aforementioned paper can diagnose single-switch faults and sensor faults, it cannot diagnose simultaneous multiple-switch faults nor intermittent switch faults. However, intermittent switch faults are actually crucial for the early warning of open-circuit faults.

This paper proposes a fault diagnosis method based on fuzzy logic reasoning that can diagnose multiple faults, including open-circuit faults, intermittent faults, and current sensor faults in power switches under nonlinear loads, with a total of 30 fault types. Even under operating conditions with fluctuating nonlinear loads, the proposed fault diagnosis method remains virtually unaffected.

(1) The characteristic patterns of open-circuit faults in three-phase four-wire inverters and the impact of nonlinear loads on voltage and current during open-circuit faults are analyzed.
(2) Fault diagnosis variables are constructed using ideal arm voltage and actual arm voltage to enable rapid detection.
(3) Trapezoidal membership functions are selected after analyzing characteristics of various membership function shapes.
(4) Diagnostic rules and tables are formulated based on fault-specific properties.
(5) An experimental setup was constructed to validate the aforementioned fault diagnosis method. The method can diagnose single-switch and same-phase bridge arm multi-switch open-circuit faults with a diagnosis time of less than 3 ms; diagnose different bridge arm multi-switch open-circuit faults with a diagnosis time of less than 5 ms; diagnose inter-switch faults with a diagnosis time of less than 1 ms; and diagnose current sensor faults with a diagnosis time of less than 4 ms. The rest of the paper is organized as follows. Section 2 designs the fault diagnostic variables. Section 3 designs the fault diagnosis scheme. Section 4 builds an experimental platform to verify the fault diagnosis scheme. Section 5 summarizes the whole paper.

2. Fault Characterization and Diagnostic Variable Design

Figure 1 illustrates the topology of a three-phase four-wire inverter with a neutral-point inductor. By incorporating an inductor at the neutral point, this topology effectively suppresses zero-sequence currents and enhances the system's adaptability to unbalanced loads, making it widely applicable in scenarios such as low-voltage distribution and distributed generation. The nonlinear load employed in this study is a typical three-phase diode rectifier load, which is extensively used in industrial rectifier units and power electronic equipment due to its simplicity, low cost, and high reliability. However, its commutation

process generates significant harmonic currents and voltage distortions, complicating inverter operating conditions and increasing fault diagnosis difficulty. Therefore, selecting this load type aligns more closely with real-world engineering fault diagnosis requirements.

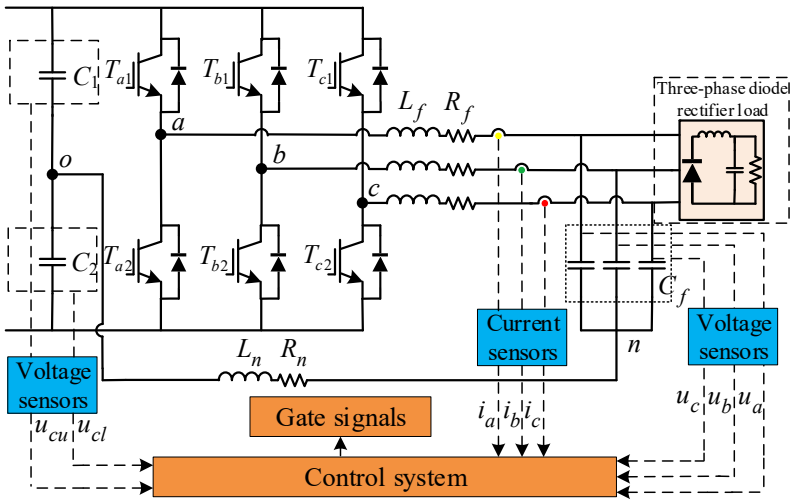


Figure 1. Three-phase four-wire inverter with neutral inductor [29].

The fault characteristics of T_{x1} ($x = a, b, c$) open-circuit faults are detailed in Figure 2. Owing to the mutual independence of the three phases in the three-phase four-wire inverter, the analysis is implemented by decomposing the inverter into a single-phase inverter with a neutral inductor. As shown in Figure 2a, during normal operation with $i_x > 0$, the current passes through path ① when T_{x1} is in the on-state; when T_{x1} is turned off, the current freewheels through diode D_{x2} along path ②. Figure 2b presents the open-circuit fault state with $i_x > 0$: at this juncture, the current only freewheels through D_{x2}, leaving only path ② operational. Figure 2c depicts the normal operation state with $i_x < 0$: when T_{x2} is conducting, the current flows via path ①; when T_{x2} is off, the current continues to freewheel through D_{x1} along path ②. In the open-circuit fault state with $i_x < 0$ (as illustrated in Figure 2d), the existence of D_{x1} renders the fault ineffective in influencing the current.

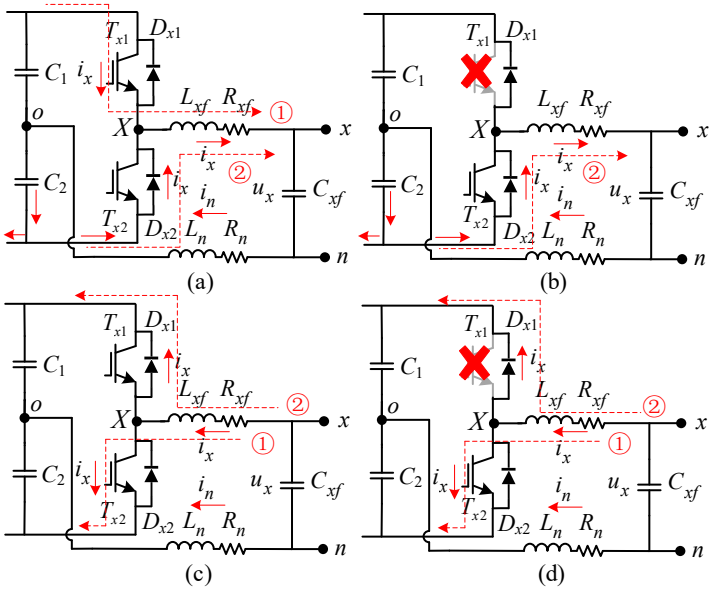


Figure 2. Demonstrates the characteristic manifestations of T_{x1} open-circuit faults, specifically covering (**a**) normal operation with $i_x > 0$, (**b**) open-circuit fault under $i_x > 0$, (**c**) normal operation with $i_x < 0$, and (**d**) open-circuit fault under $i_x < 0$.

Due to the presence of nonlinear loads, significant harmonics are generated in the bridge arm voltage and current following an open-circuit fault, as shown in Figure 3. Traditional fault diagnosis methods struggle to diagnose this operating condition. Intermittent faults are short-term open switch faults caused by loss of pulses or poor switch contact, and can be used as a warning that the switch is permanently open.

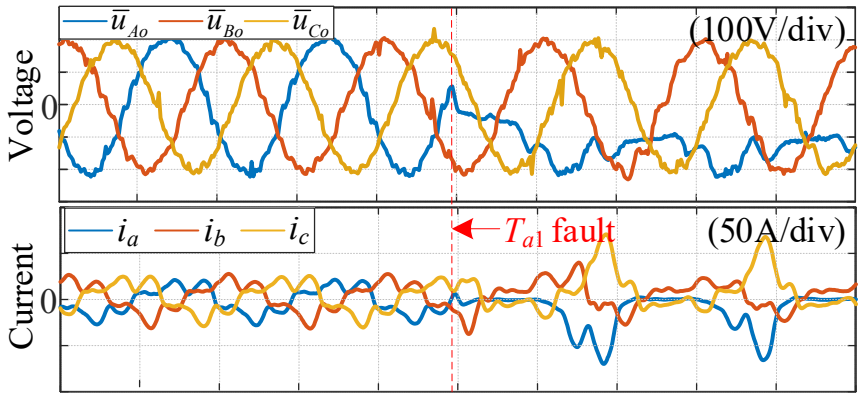


Figure 3. Three-phase four-wire inverter with neutral inductor.

When the current sensor is in the normal state, the current is measured by the current sensor as the feedback value of the inner current loop to maintain the operation of the current loop. When the current sensor has a broken wire fault, the output of the sensor is 0, which leads to the open-loop operation of the current loop, and the control system cannot obtain the current parameter and cannot realize the current control.

Taken together, the above analysis requires that the fault diagnostic variables be able to recognize both power switch open circuit and sensor faults, as well as short-duration pulse loss faults in the power switches. In addition to this, the fault diagnostic variables are required to be unaffected by harmonics before and after nonlinear load faults. The bridge arm voltage is chosen as the fault diagnostic variable, which reflects the above faults but is also affected by harmonics, spikes and ripples, which need to be handled appropriately.

From Figure 4, the average value of the ideal voltage at the midpoint of the bridge arm is calculated as

$$\overline{u}^{*}_{Xo}[k] = \frac{(u_{cu}[k]+u_{cu}[k-1])\cdot d_{x1}[k-1]}{2} - \frac{(u_{cl}[k]+u_{cl}[k-1])\cdot d_{x2}[k-1]}{2} \tag{1}$$

where $d_{x1}[k]$ denotes the actual conduction duty cycle of T_{x1} at the kth cycle and $d_{x2}[k]$ denotes the actual conduction duty cycle of T_{x2} at the kth cycle [30].

$$\overline{u}_{Xo}[k] = \frac{1}{2}(u_x[k]+u_x[k-1]) + \frac{L_{xf}}{T_s}\cdot(i_x[k]-i_x[k-1]) + \frac{R_{xf}}{2}\cdot(i_x[k]+i_x[k-1]) + \frac{L_n}{T_s}\cdot(i_n[k]-i_n[k-1]) + \frac{R_n}{2}\cdot(i_n[k]+i_n[k-1]) \tag{2}$$

$$i_n[k] = i_a[k] + i_b[k] + i_c[k] \tag{3}$$

To suppress harmonic and ripple interference, the average of the ideal bridge arm voltage and the actual bridge arm voltage must be normalized, and the normalized variable must be used as a fault diagnosis variable.

$$[|\overline{u}^{*}_{Xo}|] = \frac{\int_{t}^{t+T_{FP}} |\overline{u}^{*}_{Xo}|dt}{T_{FP}} \tag{4}$$

$$[\overline{u}_{Xo}] = \frac{\int_{t}^{t+T_{FP}} \overline{u}_{Xo} dt}{T_{FP}} \tag{5}$$

$$[|\overline{u}_{Xo}|] = \frac{\int_{t}^{t+T_{FP}} |\overline{u}_{Xo}| dt}{T_{FP}} \tag{6}$$

$$[\overline{u}_{Xo}]_n = \frac{[\overline{u}_{Xo}]}{[|\overline{u}_{Xo}|]} \tag{7}$$

$$[|\overline{u}_{Xo}|]_n = \frac{[|\overline{u}_{Xo}|]}{[|\overline{u}^*_{Xo}|]} \tag{8}$$

$$F_t = \frac{\left| C_2 \frac{du_{cl}}{dt} - C_1 \frac{du_{cu}}{dt} - (i_a + i_b + i_c) \right|}{\mu} \tag{9}$$

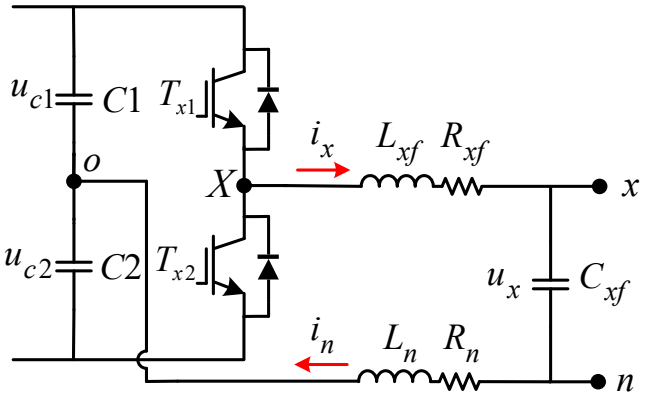


Figure 4. Single-phase simplified circuit for calculating the midpoint voltage of a bridge arm [29].

Equation (4) is the average value of the absolute value of the ideal bridge arm voltage, $|\overline{u}^*_{Xo}|$ is the absolute value of the ideal bridge arm voltage, and T_{FP} is the time of one fundamental wave period. Equation (5) is the average value of the actual bridge arm voltage. Equation (6) is the average value of the absolute value of the actual bridge arm voltage; $|\overline{u}_{Xo}|$ is the absolute value of the actual bridge arm voltage. Equation (7) is the fault diagnosis variable after normalizing the bridge arm voltage. Equation (8) is the fault diagnosis variable after normalizing the absolute value of bridge arm voltage. In Equation (9), F_t is the normalized fault differentiation variable; when $F_t > 2 - \lambda$, a sensor fault occurs, and when $F_t < \lambda$, an open-circuit fault occurs. μ is the fault differentiation threshold.

The use of bridge arm voltage averages mitigates harmonic and ripple disturbances, and normalization of bridge arm voltages avoids fluctuations in fault diagnostic variables caused by voltage fluctuations, and also facilitates subsequent fuzzy logic-based fault diagnostic schemes.

3. Fault Diagnosis Scheme Based on Fuzzy Logic

Fuzzy logic reasoning consists of 3 main parts: fuzzification, fuzzy inference and defuzzification. The fuzzy membership function used in this fault diagnosis method is a trapezoidal function. Due to the presence of nonlinear loads and sampling noise, the measured data generally contain noise and harmonic interference. Since the membership value in the flat-top segment is fixed at 1, the membership value remains unchanged when the indicator fluctuates slightly near the pass/fail threshold, and the fuzzy output remains

stable. This effectively mitigates data fluctuations caused by harmonics, noise, and random measurement disturbances.

$$X_n = \begin{cases} H = \begin{cases} 1, & [\overline{u}_{Xo}]_n < -0.1 \\ \frac{1}{\alpha-0.1}[\overline{u}_{Xo}]_n + \frac{\alpha}{\alpha-0.1}, & -0.1 \le [\overline{u}_{Xo}]_n < -\alpha \end{cases} \\ HI = \begin{cases} \frac{-1}{\alpha-0.1}[\overline{u}_{Xo}]_n + \frac{-0.1}{\alpha-0.1}, & -0.1 \le [\overline{u}_{Xo}]_n < -\alpha \\ 1, & -\alpha \le [\overline{u}_{Xo}]_n < -\beta \\ \frac{1}{\alpha-0.1}[\overline{u}_{Xo}]_n + \frac{\alpha+\beta-0.1}{\alpha-0.1}, & -\beta \le [\overline{u}_{Xo}]_n < 0.1-\alpha-\beta \end{cases} \\ N = \begin{cases} \frac{-1}{\alpha-0.1}[\overline{u}_{Xo}]_n + \frac{\beta}{\alpha-0.1}, & -\beta \le [\overline{u}_{Xo}]_n < 0.1-\alpha-\beta \\ 1, & 0.1-\alpha-\beta \le [\overline{u}_{Xo}]_n < \alpha+\beta-0.1 \\ \frac{1}{\alpha-0.1}[\overline{u}_{Xo}]_n + \frac{\beta-0.1}{\alpha-0.1}, & \alpha+\beta-0.1 \le [\overline{u}_{Xo}]_n < \beta \end{cases} \\ LI = \begin{cases} \frac{-1}{\alpha-0.1}[\overline{u}_{Xo}]_n + \frac{\alpha+\beta-0.1}{\alpha-0.1}, & \alpha+\beta-0.1 \le [\overline{u}_{Xo}]_n < \beta \\ 1, & \beta \le [\overline{u}_{Xo}]_n < 0.1-\alpha \\ \frac{1}{\alpha-0.1}[\overline{u}_{Xo}]_n + \frac{-0.1}{\alpha-0.1}, & 0.1-\alpha \le [\overline{u}_{Xo}]_n < 0.1 \end{cases} \\ L = \begin{cases} \frac{-1}{\alpha-0.1}[\overline{u}_{Xo}]_n + \frac{\alpha}{\alpha-0.1}, & 0.1-\alpha \le [\overline{u}_{Xo}]_n < 0.1 \\ 1, & 0.1 \le [\overline{u}_{Xo}]_n \end{cases} \end{cases} \tag{10}$$

where α = 0.08, and β = 0.05. The faults to be diagnosed include single and multi-switch open-circuit faults, intermittent faults and current sensor faults. Especially in the case of multi-switch faults, the faulty switches interact with each other, so the threshold set based on a single switch is difficult to adapt to the multi-switch case, so the threshold α is set by extensive experiments. Due to the presence of voltage harmonics and ripples, the proposed fault diagnosis variables may fluctuate in a small range, and the threshold β can avoid the misdiagnosis caused by the above reasons.

$$Y_n = \begin{cases} H = \begin{cases} 1, & [|\overline{u}_{Xo}|]_n < \gamma \\ \frac{1}{2\gamma-2}[|\overline{u}_{Xo}|]_n + \frac{\gamma-2}{2\gamma-2}, & \gamma \le [|\overline{u}_{Xo}|]_n < 2-\gamma \\ 0, & 2-\gamma \le [|\overline{u}_{Xo}|]_n \end{cases} \\ L = \begin{cases} 0, & [|\overline{u}_{Xo}|]_n < \gamma \\ \frac{-1}{2\gamma-2}[|\overline{u}_{Xo}|]_n + \frac{\gamma}{2\gamma-2}, & \gamma \le [|\overline{u}_{Xo}|]_n < 2-\gamma \\ 1, & 2-\gamma \le [|\overline{u}_{Xo}|]_n \end{cases} \end{cases} \tag{11}$$

The fault diagnostic variable Y_n is mainly used to determine whether an open-circuit fault has occurred in a power switch of the same bridge arm. When an open-circuit fault occurs in a switch of the same bridge arm, the switch will no longer conduct. At this time, the presence of the diode makes the bridge arm still have voltage, and the voltage is still a sinusoidal waveform, but the voltage value is very small. The size of the voltage value is mainly determined by the voltage of the phase current in the filter inductance and the neutral current in the neutral inductance. Therefore, set γ = 0.95.

$$Z_n = \begin{cases} H = \begin{cases} 1, & F_t < \lambda \\ \frac{1}{2\lambda-2}F_t + \frac{\lambda-2}{2\lambda-2}, & \lambda \le F_t < 2-\lambda \\ 0, & 2-\lambda \le F_t \end{cases} \\ L = \begin{cases} 0, & F_t < \lambda \\ \frac{-1}{2\lambda-2}F_t + \frac{\lambda}{2\lambda-2}, & \lambda \le F_t < 2-\lambda \\ 1, & 2-\lambda \le F_t \end{cases} \end{cases} \tag{12}$$

The fault detection variable Z_n is mainly used to differentiate between power switch open circuits, intermittent faults and sensor faults, $\lambda = 0.99$. From the above analysis, the input affiliation function of the fuzzy logic system, as shown in Figure 5, can be obtained.

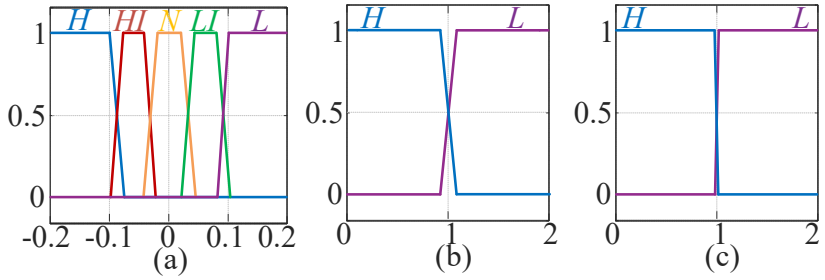


Figure 5. Membership input functions for fuzzy logic reasoning. (**a**) X_n. (**b**) Y_n. (**c**) Z_n.

The relationship between inputs and outputs can be expressed by the IF-THEN rule, and the rules for determining open circuit, intermittent faults, and sensor faults are given below, using phase A as an example.

(1) IF $X_a = H$ and $Z = H$, THEN T_{a1} open-circuit fault, T_{a2} and sensor A normal.
(2) IF $X_a = L$ and $Z = H$, THEN T_{a2} open-circuit fault, T_{a1} and sensor A normal.
(3) IF $X_a = HI$ and $Z = H$, THEN T_{a1} intermittent fault, T_{a2} and sensor A normal.
(4) IF $X_a = LI$ and $Z = H$, THEN T_{a2} intermittent fault, T_{a1} and sensor A normal.
(5) IF $Y_a = H$ and $Z = H$, THEN T_{a1} and T_{a2} open-circuit fault, sensor A normal.
(6) IF $X_a = HI$ or $X_a = LI$ and $Z = L$, THEN sensor A fault.
(7) IF $X_a = N$ and $Y_a = N$, THEN T_{a1}, T_{a2} and sensor A normal.

By analyzing the above rules, the kinds of fault diagnosis based on fuzzy logic are obtained, as shown in Table 1.

Table 1. Types of fault diagnosis based on fuzzy logic.

Fault Type		X_a	X_b	X_c	Y_a	Y_b	Y_c	Z
Open-circuit fault	T_{a1}	H	N	N	L	L	L	H
	T_{a2}	N	L	N	L	L	L	H
	T_{b1}	N	H	N	L	L	L	H
	T_{b2}	N	L	N	L	L	L	H
	T_{c1}	N	N	H	L	L	L	H
	T_{c2}	N	N	L	L	L	L	H
	T_{a1}, T_{a2}	N	N	N	H	L	L	H
	T_{b1}, T_{b2}	N	N	N	L	H	L	H
	T_{c1}, T_{c2}	N	N	N	L	L	H	H
	T_{a1}, T_{b1}	H	H	N	L	L	L	H
	T_{a1}, T_{c1}	H	N	H	L	L	L	H
	T_{b1}, T_{c1}	N	H	H	L	L	L	H
	T_{a2}, T_{b2}	L	L	N	L	L	L	H
	T_{a2}, T_{c2}	L	N	L	L	L	L	H
	T_{b2}, T_{c2}	N	L	L	L	L	L	H
	T_{a1}, T_{b2}	H	L	N	L	L	L	H
	T_{a1}, T_{c2}	H	N	L	L	L	L	H
	T_{a2}, T_{b1}	L	H	N	L	L	L	H
	T_{a2}, T_{c1}	L	N	H	L	L	L	H
	T_{b1}, T_{c2}	N	H	L	L	L	L	H
	T_{b2}, T_{c1}	N	L	H	L	L	L	H

Table 1. *Cont.*

Fault Type		X_a	X_b	X_c	Y_a	Y_b	Y_c	Z
Intermittent fault	T_{a1}	HI	N	N	L	L	L	H
	T_{a2}	LI	N	N	L	L	L	H
	T_{b1}	N	HI	N	L	L	L	H
	T_{b2}	N	LI	N	L	L	L	H
	T_{c1}	N	N	HI	L	L	L	H
	T_{c2}	N	N	LI	L	L	L	H
Sensor fault	Sensor A	HI, LI	N	N	L	L	L	L
	Sensor B	N	HI, LI	N	L	L	L	L
	Sensor C	N	N	HI, LI	L	L	L	L

4. Verification

The proposed fault diagnosis method is verified by building an experimental bench, which is shown in Figure 6. The test bench consists of a DC power supply, intelligent power module, rectifier-type load units, multiple sensors and passive filtering components. Its digital control framework adopts a digital signal processor (DSP) plus complex programmable logic device (CPLD) architecture. The DSP's main CPU executes control routines, while its control law accelerator (CLA) core is specially assigned for real-time fault diagnosis algorithms. The parameters of the experimental bench are shown in Table 2.

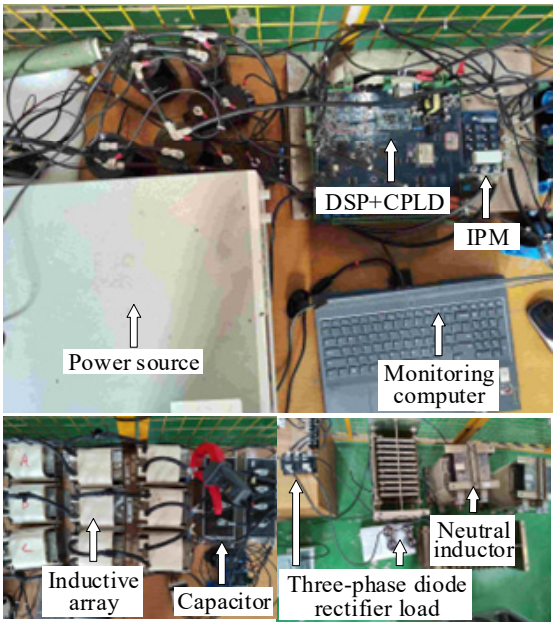


Figure 6. Experimental platform of three-phase four-wire inverter.

Figure 7 shows the diagnostic test results for the T_{a1} open-circuit fault. Prior to the fault occurrence, the presence of nonlinear loads caused harmonics to appear in the three-phase bridge arm voltages while maintaining a 120-degree phase angle. After the open-circuit fault, influenced by the nonlinear load, the faulted phase voltage could not maintain a half-wave state, and the non-faulted voltage also generated significant harmonics. The fault detection flag $[\overline{u}_{Ao}]_n$ rapidly decreased. When $[\overline{u}_{Ao}]_n$ fell below $-\alpha$, the fault occurrence was determined. At this point, the fault type determination flag Ft was less than 1, indicating an open-circuit fault had occurred. The faulty switch was identified as T_{a1}, and the entire fault diagnosis time was less than 2 ms.

Table 2. Four-wire inverter's parameters.

Parameter	Symbol	Value
DC voltage	u_{cu}, u_{cl}	250 V
Inductor current	$i_{a,\,b,\,c}$	15 A_{RMS}
Filter inductance	L_f (R_f)	0.3 mH
Output voltage	$u_{a,\,b,\,c}$	200 V_p
Neutral inductance	L_n (R_n)	0.6 mH
Output voltage	$u_{a,\,b,\,c}$	200 V_p
Switching frequency	f_w	2.5 kHz
Fault diagnosis type threshold	λ	8
Sampling frequency	f_s	5 kHz
Frequency of fault diagnosis	f_d	5 kHz

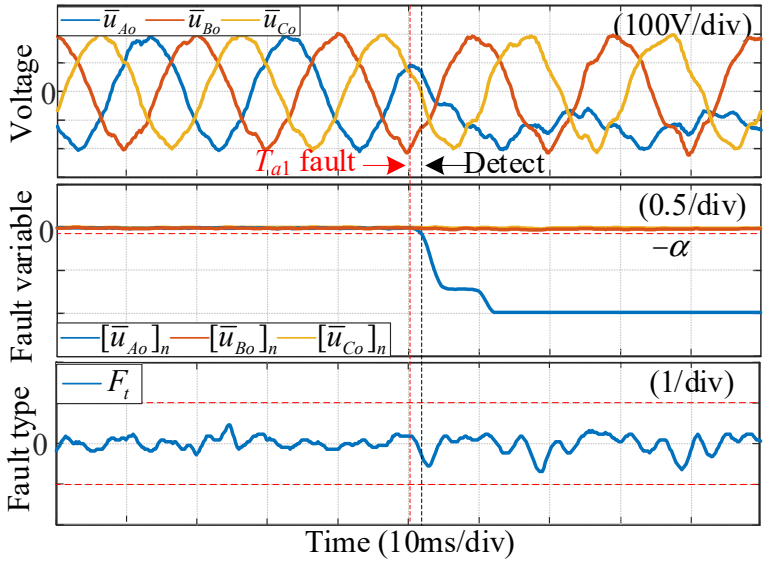


Figure 7. Experiments for T_{a1} open-circuit fault.

Figure 8 shows the diagnostic test results for simultaneous open-circuit faults in T_{a1} and T_{b1}. After the open-circuit faults occur, the fault detection indicators $[\overline{u}_{Ao}]_n$ and $[\overline{u}_{Bo}]_n$ rapidly decrease. When $[\overline{u}_{Ao}]_n$ and $[\overline{u}_{Bo}]_n$ fall below $-\alpha$, a fault is determined to have occurred. At this point, the fault type determination flag F_t is less than 1, indicating an open-circuit fault has occurred. The faulty switches are T_{a1} and T_{b1}, with the entire fault diagnosis time being less than 4 ms. It should be noted that the T_{b1} open-circuit fault occurred during its negative half-cycle, yet the proposed fault diagnosis method still accurately completed the diagnosis—an advantage not possessed by traditional methods. Furthermore, this experiment demonstrates that the proposed fault diagnosis method can diagnose open-circuit faults occurring simultaneously in the same half-bridge.

Figure 9 shows the diagnostic test results for simultaneous open-circuit faults in T_{a1} and T_{b2}. After the open-circuit faults occur, the fault detection indicator $[\overline{u}_{Ao}]_n$ rapidly decreases, while $[\overline{u}_{Bo}]_n$ rapidly increases. When $[\overline{u}_{Ao}]_n$ falls below $-\alpha$ and $[\overline{u}_{Bo}]_n$ exceeds α, a fault is determined to have occurred. At this point, the fault type identification flag F_t is less than 1, indicating an open-circuit fault has occurred. The faulty switches are T_{a1} and T_{b2}, with the entire fault diagnosis process completed in less than 6 ms. Although nonlinear loads cause a significant increase in voltage distortion in the non-faulted phase C, the proposed fault diagnosis method remains effective and exhibits strong robustness to harmonic variations. Furthermore, this experiment demonstrates that the proposed fault

diagnosis method can diagnose open-circuit faults occurring simultaneously in different bridge arms.

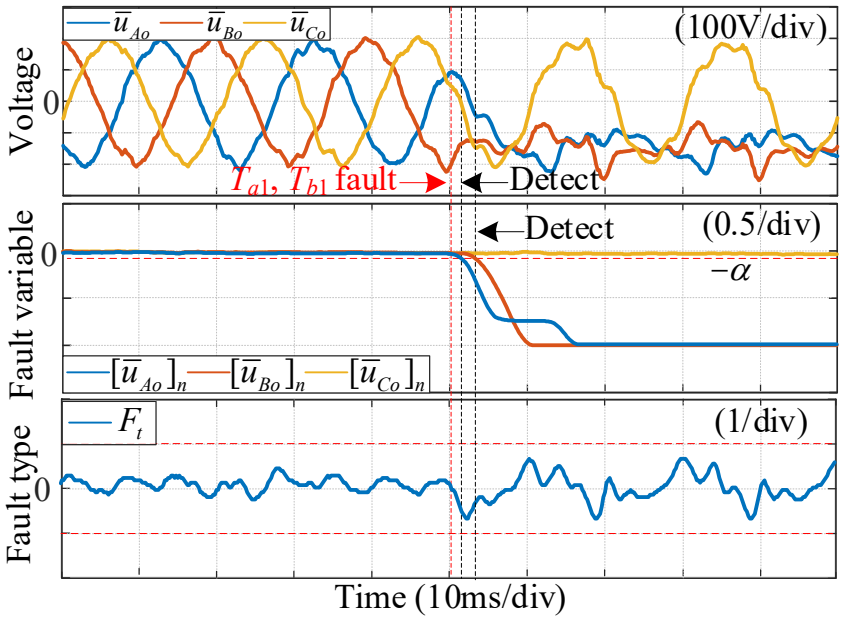


Figure 8. Experiments for T_{a1} and T_{b1} open-circuit fault.

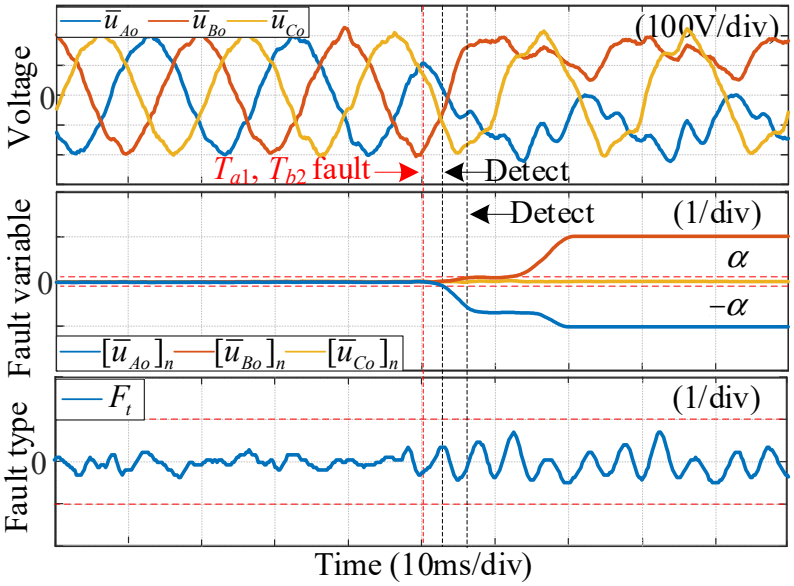


Figure 9. Experiments for T_{a1} and T_{b2} open-circuit fault.

Figure 10 shows the diagnostic test results for simultaneous open-circuit faults in T_{a1} and T_{a2}. After the open-circuit fault occurs, the fault detection indicator x rapidly decreases. When $[\overline{u}_{Ao}]_n$ falls below $-\gamma$, a fault is determined to have occurred. At this point, the fault type determination indicator F_t is less than 1, indicating an open-circuit fault has occurred. The faulty switches are T_{a1} and T_{a2}, with the entire fault diagnosis time being less than 2 ms. It can be seen that the proposed fault diagnosis method is capable of detecting this fault very quickly. Compared to multiple-switch faults occurring on different bridge arms, multiple-switch faults occurring on the same bridge arm can be detected simultaneously, and the detection time is roughly equivalent to that of a single-switch fault. This experiment demonstrates that the proposed fault diagnosis method can detect simultaneous open-circuit faults occurring in the same circuit.

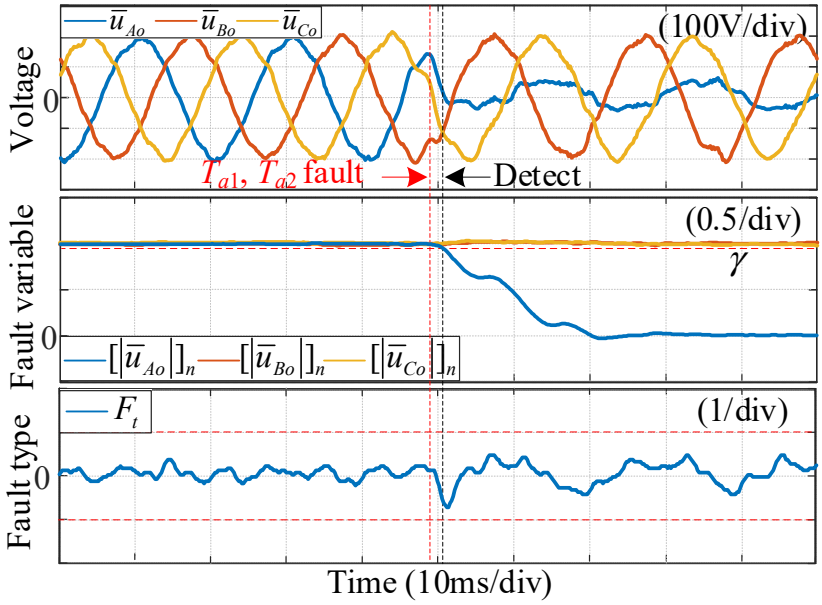


Figure 10. Experiments for T_{a1} and T_{a2} open-circuit fault.

Figure 11 displays the diagnostic results for a phase C current sensor disconnection fault, where the current sensor sampling value reads zero after the fault occurs. The presence of inductance causes changes in the bridge arm voltage configuration. At this point, $[\overline{u}_{Co}]_n$ rapidly increases. When $[\overline{u}_{Co}]_n$ exceeds α, a fault is determined to have occurred. Since the fault type indicator F_t is greater than 1, a sensor fault is identified, with the fault diagnosis time being less than 4 ms. After confirming the sensor fault, the faulty sensor is reconstructed using Equation (25) from [30].

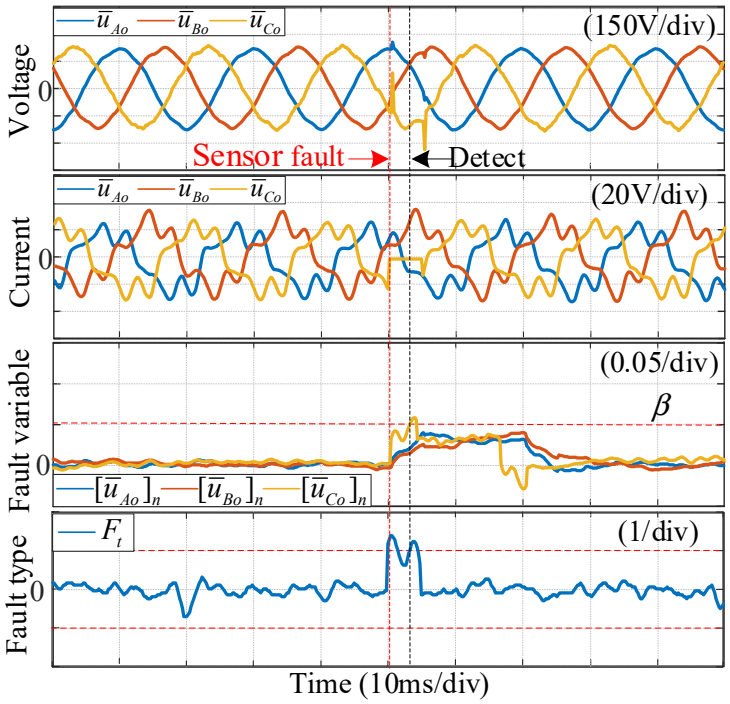


Figure 11. Experiments for phase-A current sensor fault.

Figure 12 shows the diagnostic results for an intermittent fault in T_{c1} (fault duration: 2 switching cycles). After the intermittent fault in T_{c1} occurs, $[\overline{u}_{Co}]_n$ rapidly decreases. When $[\overline{u}_{Co}]_n$ falls below $-\beta$, a fault is detected. At this point, F_t is less than 1, confirming

an intermittent fault. The entire fault diagnosis process takes less than 0.5 ms. Considering the experimental switching frequency of 2.5 kHz, this indicates that intermittent faults are detected immediately upon occurrence. Experimental results demonstrate that this method can diagnose intermittent faults, but the fault duration should not be excessively long, otherwise it may be misclassified as an open-circuit fault.

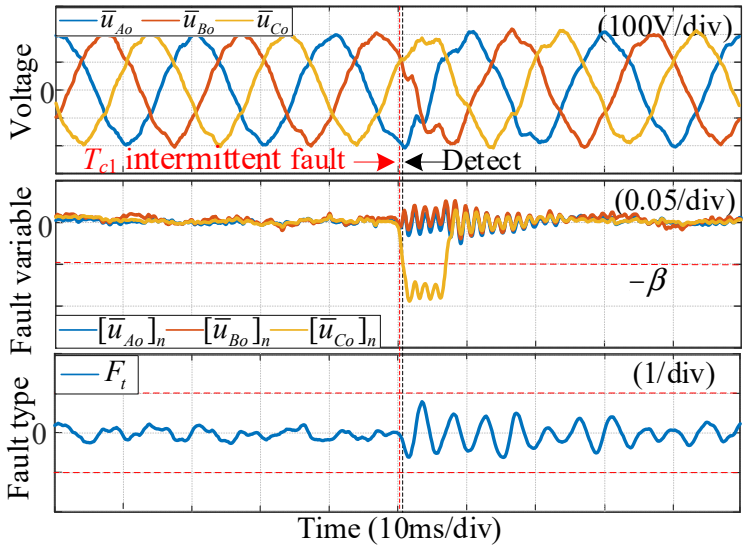


Figure 12. Experiments for T_{c1} intermittent fault.

Figure 13 presents experimental results demonstrating the impact of voltage sampling noise on open-circuit fault diagnosis, with a maximum noise amplitude of 40 V. Following the occurrence of an open-circuit fault in T_{b1}, the fault detection variable $[\overline{u}_{Bo}]_n$ rapidly decreases. When $[\overline{u}_{Bo}]_n$ falls below the threshold $-\alpha$, a fault is determined to have occurred. At this point, the fault classification variable F_t is less than 1, indicating an open-circuit fault in T_{b1}. This experiment demonstrates that noise interference does not affect the proposed fault diagnosis method.

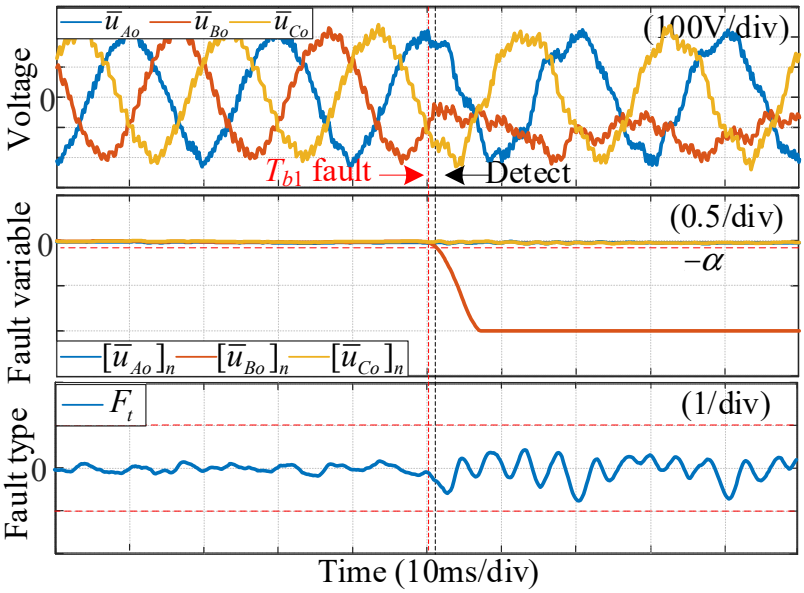


Figure 13. Experiments on the effect of noise on fault diagnosis.

Figures 14 and 15 illustrate the impact of 50% load engagement and disengagement on fault diagnosis. Although the fault diagnosis variable fluctuates slightly during load

engagement and disengagement, it remains above the threshold. This demonstrates that the proposed fault diagnosis method exhibits strong robustness against load fluctuations.

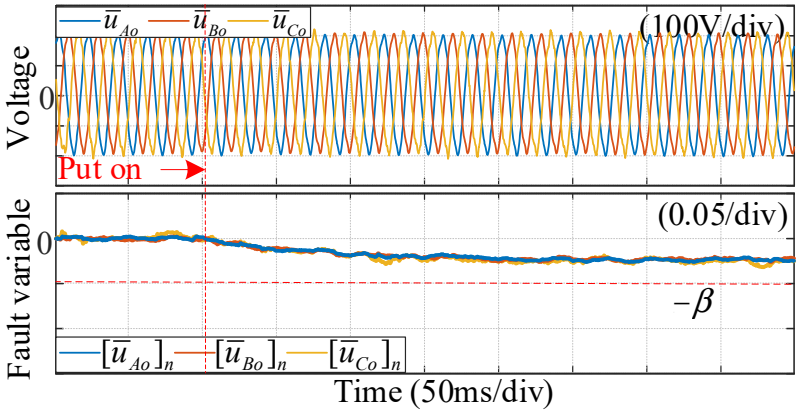


Figure 14. Experiments on the effect of load put on fault diagnosis.

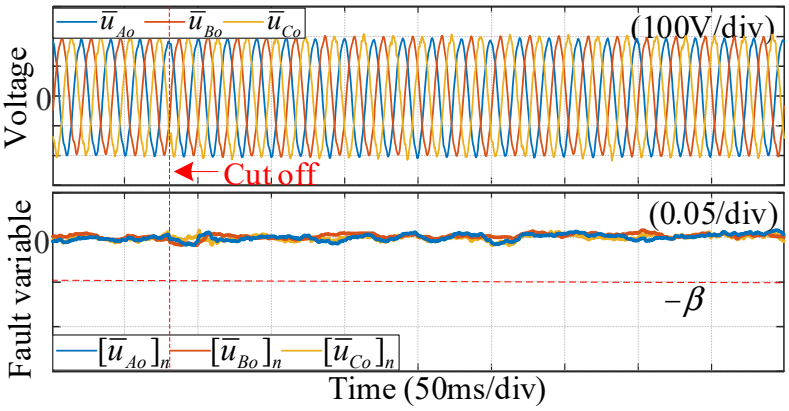


Figure 15. Experiments on the effect of load cut off fault diagnosis.

To show the advantages of the proposed fault diagnosis method, we have compared it with other methods as shown in Table 3. Reference [31] employs multi-state data processing and artificial neural network methods to diagnose open-circuit faults in multi-switch systems. However, this method requires a large amount of data for offline training, involves excessive diagnostic time, and is highly complex. Reference [32] employs the discrete Fourier transform and principal component analysis to diagnose open-circuit faults. This method requires a large amount of data and generally has a moderate diagnostic speed. Reference [33] achieves open-circuit fault diagnosis by extracting abnormal current waveform patterns caused by open-circuit faults in the corresponding switch. While this method offers relatively fast diagnosis, it is susceptible to load fluctuations. Reference [34] employs a support vector machine and transfer learning algorithms to diagnose open-circuit faults. Since this method is data-driven, it requires a large amount of data and results in slow diagnostic speeds. Reference [12] implements open-circuit fault diagnosis based on the average phase voltage model. While this method offers fast diagnosis, it lacks robustness against load fluctuations and is difficult to apply to systems with nonlinear loads. As shown in Table 3, the proposed fault diagnosis scheme is capable of diagnosing open-circuit faults, intermittent faults, and current sensor faults. This scheme can diagnose both single-point faults and multiple parallel faults. This fault diagnosis method does not require the addition of an extra data acquisition system or the prior collection of large amounts of data, and it enables online simultaneous diagnosis of multiple faults.

Table 3. Comparison with other methods.

Method	Plant	Detection Variable	Faulty Type	Detection Time	Load Type	Data for Diagnosis	Complexity
[31]	Three-phase inverter	Three-phase currents	Open-circuit	<2 FP	Resistance	Large	High
[32]	Three-phase inverter	Three-phase currents	Open-circuit	<0.5 FP	Induction motor	Medium	Large
[33]	Three-phase inverter	Three-phase currents	Open-circuit	<0.2 FP	Resistance	Less	Medium
[34]	Three-phase inverter	Three-phase currents; Three-phase voltages	Open-circuit	<2 FP	--	Large	High
[12]	Three-phase inverter	Three-phase currents; Three-phase voltages	Open-circuit	<0.15 FP	Resistance	Less	High
Proposed method	Three-phase four-wire inverter	Three-phase currents; Three-phase voltages	Open-circuit, Intermittent, sensor fault	<0.15 FP	Three-phase diode rectifier	Less	Medium

Note: FP represents the fundamental period.

5. Conclusions

This paper proposes a diagnostic method based on fuzzy logic for detecting open-circuit, intermittent, and current sensor disconnection faults in three-phase four-wire inverters. First, the open-circuit fault characteristics of four-wire inverters and the impact of nonlinear loads on open-circuit fault diagnosis are analyzed. Next, fault diagnosis variables are constructed using the ideal and actual arm voltages. Subsequently, fuzzy logic is employed for fault classification and diagnosis. Finally, an experimental setup is constructed to validate the proposed fault diagnosis method.

The proposed fault diagnosis scheme can diagnose open circuit, intermittent fault and current sensor faults. It can diagnose single fault and multiple simultaneous faults. The diagnosis time for open-circuit and current sensor fault are less than 4 ms; for intermittent fault, it is less than 1 ms. The proposed fault diagnosis method neither requires the addition of an extra acquisition system nor the acquisition of a large amount of data in advance, realizing the simultaneous online diagnosis of multiple faults.

Author Contributions: Conceptualization, J.H. and Y.S.; methodology, Y.S.; software, Y.S.; validation, H.F., Z.Y. and C.Z.; formal analysis, Y.S.; investigation, K.C.; resources, H.F.; data curation, Z.Y.; writing—original draft preparation, C.Z. and G.W.; writing—review and editing, Y.S.; visualization, K.C. and G.W.; supervision, H.F.; project administration, J.H.; funding acquisition, J.H. All authors have read and agreed to the published version of the manuscript.

Funding: This work was supported by the National Natural Science Foundation of China (NSFC) under Grant 52175038.

Data Availability Statement: The data presented in this study are available within the article.

Conflicts of Interest: The authors declare no conflicts of interest.

References

1. Dai, M.; Marwali, M.N.; Jung, J.-W.; Keyhani, A. A Three-Phase Four-Wire Inverter Control Technique for a Single Distributed Generation Unit in Island Mode. *IEEE Trans. Power Electron.* **2008**, *23*, 322–331.
2. Zhang, H.; da Sun, C.; Li, Z.-X.; Liu, J.; Cao, H.-Y.; Zhang, X. Voltage Vector Error Fault Diagnosis for Open-Circuit Faults of Three-Phase Four-Wire Active Power Filters. *IEEE Trans. Power Electron.* **2017**, *32*, 2215–2226.
3. Chen, J.; Diao, L.-J.; Wang, L.; Du, H.; Liu, Z. Distributed Auxiliary Inverter of Urban Rail Train and Current Control Strategy under Complicated Load Condition. *IEEE Trans. Power Electron.* **2016**, *31*, 1745–1756. [CrossRef]
4. Yang, S.Y.; Bryant, A.T.; Mawby, P.A.; Xiang, D.; Ran, L.; Tavner, P.J. An Industry-Based Survey of Reliability in Power Electronic Converters. *IEEE Trans. Ind. Appl.* **2011**, *47*, 1441–1451. [CrossRef]
5. Yu, Y.; Li, H.; Yao, R.; Iannuzzo, F.; Zhu, Z.; Chen, X. Short-Circuit Capability Optimization of Press-Pack IGBT by Improving Active Edge Heat Dissipation. *IEEE Trans. Power Electron.* **2023**, *38*, 6143–6156. [CrossRef]
6. Mirafzal, B. Survey of Fault-Tolerance Techniques for Three-Phase Voltage Source Inverters. *IEEE Trans. Ind. Electron.* **2014**, *61*, 5192–5202. [CrossRef]
7. Masri, B.; Al Sheikh, H.; Karami, N.; Kanaan, H.Y.; Moubayed, N. A Review on Artificial Intelligence Based Strategies for Open-Circuit Switch Fault Detection in Multilevel Inverters. In Proceedings of the IECON 2021-47th Annual Conference of the IEEE Industrial Electronics Society, Toronto, ON, Canada, 13–16 October 2021; pp. 1–8.
8. Xing, Z.; He, Y.; Zhang, W. An Online Multiple Open-Switch Fault Diagnosis Method for T-Type Three-Level Inverters Based on Multi-modal Deep Residual Filter Network. *IEEE Trans. Ind. Electron.* **2023**, *70*, 10669–10679.
9. Gou, B.; Xu, Y.; Xia, Y.; Deng, Q.; Ge, X. An Online Data-Driven Method for Simultaneous Diagnosis of IGBT and Current Sensor Fault of Three-Phase PWM Inverter in Induction Motor Drives. *IEEE Trans. Power Electron.* **2020**, *35*, 13281–13294. [CrossRef]
10. Xia, Y.; Xu, Y. A Transferrable Data-Driven Method for IGBT Open-Circuit Fault Diagnosis in Three-Phase Inverters. *IEEE Trans. Power Electron.* **2021**, *36*, 13478–13488. [CrossRef]
11. Li, Z.; Wheeler, P.; Watson, A.; Costabeber, A.; Wang, B.; Ren, Y.; Bai, Z.; Ma, H. A Fast Diagnosis Method for Both IGBT Faults and Current Sensor Faults in Grid-Tied Three-Phase Inverters with Two Current Sensors. *IEEE Trans. Power Electron.* **2020**, *35*, 5267–5527. [CrossRef]
12. Zhang, W.; He, Y.; Wang, C.; Chen, M.; Sui, C. A Multiple Open-Circuit Fault Diagnosis Method for Two-Level Three-Phase Voltage Source Converters Based on Average-Phase Voltage Model. *IEEE J. Emerg. Sel. Top. Power Electron.* **2022**, *10*, 1138–1152. [CrossRef]
13. Zhang, W.; He, Y. A Hypothesis Method for T-Type Three-Level Inverters Open-Circuit Fault Diagnosis Based on Output Phase Voltage Model. *IEEE Trans. Power Electron.* **2022**, *37*, 9718–9732. [CrossRef]
14. Zhang, W.; He, Y.; Chen, J. A Robust Open-Circuit Fault Diagnosis Method for Three-Level T-Type Inverters Based on Phase Voltage Vector Residual Under Modulation Mode Switching. *IEEE Trans. Power Electron.* **2023**, *38*, 5309–5322.
15. Wu, Z.; Zhao, J.; Luo, H.; Liu, Y. Real-Time Open-Circuit Fault Diagnosis Method for T-Type Rectifiers Based on Median Current Analysis. *IEEE Trans. Power Electron.* **2023**, *38*, 8956–8965. [CrossRef]
16. Wu, F.; Zhao, J. Current Similarity Analysis-Based Open-Circuit Fault Diagnosis for Two-Level Three-Phase PWM Rectifier. *IEEE Trans. Power Electron.* **2017**, *32*, 3935–3945.
17. Zhuo, S.; Gaillard, A.; Xu, L.; Liu, C.; Paire, D.; Gao, F. An Observer Based Switch Open-Circuit Fault Diagnosis of DC–DC Converter for Fuel Cell Application. *IEEE Trans. Ind. Appl.* **2020**, *56*, 3159–3167. [CrossRef]
18. Xu, S.; Huang, W.; Wang, H.; Zheng, W.; Wang, J.; Chai, Y.; Ma, M. A Simultaneous Diagnosis Method for Power Switch and Current Sensor Faults in Grid-Connected Three-Level NPC Inverters. *IEEE Trans. Power Electron.* **2023**, *38*, 1104–1118. [CrossRef]
19. Wang, T.; Liang, L.; Hao, Z.; Monti, A.; Ponci, F. LPV Model-Based Fault Detection and Isolation in DC Microgrids Through Signature Recognition. *IEEE Trans. Smart Grid.* **2023**, *14*, 2558–2571. [CrossRef]
20. Ma, G.; Zhang, H.; Sun, Z.; Yao, C.; Ren, G.; Xu, S. Current Sensor Fault Localization and Identification of PMSM Drives Using Difference Operator. *IEEE J. Emerg. Sel. Top. Power Electron.* **2023**, *11*, 1097–1110. [CrossRef]
21. Yu, Y.; Zhao, Y.; Wang, B.; Huang, X.; Xu, D. Current Sensor Fault Diagnosis and Tolerant Control for VSI-Based Induction Motor Drives. *IEEE Trans. Power Electron.* **2018**, *33*, 4238–4248. [CrossRef]
22. Wu, C.; Guo, C.; Xie, Z.; Ni, F.; Liu, H. A Signal-Based Fault Detection and Tolerance Control Method of Current Sensor for PMSM Drive. *IEEE Trans. Ind. Electron.* **2018**, *65*, 9646–9657. [CrossRef]
23. Jlassi, I.; Estima, J.O.; El Khil, S.K.; Bellaaj, N.M.; Cardoso, A.J.M. A Robust Observer-Based Method for IGBTs and Current Sensors Fault Diagnosis in Voltage-Source Inverters of PMSM Drives. *IEEE Trans. Ind. Appl.* **2017**, *53*, 2894–2905. [CrossRef]
24. Jlassi, I.; Cardoso, A.J.M. A Single Method for Multiple IGBT, Current, and Speed Sensor Faults Diagnosis in Regenerative PMSM Drives. *IEEE J. Emerg. Sel. Top. Power Electron.* **2020**, *8*, 2583–2599. [CrossRef]
25. Xu, S.; Huang, W.; Huang, D.; Chen, H.; Chai, Y.; Ma, M.; Zheng, W.X. A Reduced-Order Observer-Based Method for Simultaneous Diagnosis of Open-Switch and Current Sensor Faults of a Grid-Tied NPC Inverter. *IEEE Trans. Power Electron.* **2023**, *38*, 9019–9032. [CrossRef]

26. Wang, X.; Wang, Z.; Xu, Z.; Cheng, M.; Wang, W.; Hu, Y. Comprehensive Diagnosis and Tolerance Strategies for Electrical Faults and Sensor Faults in Dual Three-Phase PMSM Drives. *IEEE Trans. Power Electron.* **2019**, *34*, 6669–6684. [CrossRef]
27. Yao, W.; Xu, Y.; Tang, Y.; Loh, P.C.; Zhang, X.; Blaabjerg, F. Generalized Power Decoupling Control for Single-Phase Differential Inverters With Nonlinear Loads. *IEEE J. Emerg. Sel. Top. Power Electron.* **2019**, *7*, 1137–1151. [CrossRef]
28. Cao, H.; Wang, F.; Liu, J. Analysis of Fast-Scale Instability in Three-Level T-Type Single-Phase Inverter Feeding Diode-Bridge Rectifier With Inductive Load. *IEEE Trans. Power Electron.* **2022**, *37*, 15066–15083. [CrossRef]
29. Sun, Y.; Chen, J.; Dai, X.; Qiu, R. Noninvasive condition monitoring of three-phase four-wire inverter system parameters. *Int. J. Electr. Power Energy Syst.* **2024**, *162*, 110329. [CrossRef]
30. Sun, Y.; Chen, J.; Qiu, R.; Li, C. Open-Circuit, Current Sensor Fault Diagnosis of Three-Phase Four-Wire Inverters Based on Fourier Fitting. *IEEE Trans. Instrum. Meas.* **2024**, *73*, 3522813. [CrossRef]
31. Huang, Z.; Wang, Z.; Zhang, H. Multiple Open-Circuit Fault Diagnosis Based on Multistate Data Processing and Subsection Fluctuation Analysis for Photovoltaic Inverter. *IEEE Trans. Instrum. Meas.* **2018**, *67*, 516–526. [CrossRef]
32. Sun, X.; Song, C.; Zhang, Y.; Sha, X.; Diao, N. An Open-Circuit Fault Diagnosis Algorithm Based on Signal Normalization Preprocessing for Motor Drive Inverter. *IEEE Trans. Instrum. Meas.* **2023**, *72*, 3513712. [CrossRef]
33. Luo, Y.; Zhang, L.; Chen, C.; Li, K.; Li, K. Real-Time Diagnosis of Open Circuit Faults in Three-Phase Voltage Source Inverters. *IEEE Trans. Power Electron.* **2024**, *39*, 7572–7585.
34. Xia, Y.; Xu, Y.; Zhou, N. A Transferrable and Noise-Tolerant Data-Driven Method for Open-Circuit Fault Diagnosis of Multiple Inverters in a Microgrid. *IEEE Trans. Ind. Electron.* **2024**, *71*, 8017–8027. [CrossRef]

Disclaimer/Publisher's Note: The statements, opinions and data contained in all publications are solely those of the individual author(s) and contributor(s) and not of MDPI and/or the editor(s). MDPI and/or the editor(s) disclaim responsibility for any injury to people or property resulting from any ideas, methods, instructions or products referred to in the content.